

Transport and Strong-Correlation Phenomena in Carbon Nanotube Quantum Dots in a Magnetic Field

M. Mizuno¹, Eugene H. Kim¹ and G. B. Martins²

¹ *Department of Physics, University of Windsor, Windsor, Ontario, Canada N9B 3P4*

² *Department of Physics, Oakland University, Rochester, Michigan 48309*

Transport through carbon nanotube (CNT) quantum dots (QDs) in a magnetic field is discussed. The evolution of the system from the ultraviolet to the infrared is analyzed; the strongly correlated (SC) states arising in the infrared are investigated. Experimental consequences of the physics are presented — the SC states arising at various fillings are shown to be drastically different, with distinct signatures in the conductance and, in particular, the noise. Besides CNT QDs, our results are also relevant to double QD systems.

Since their discovery, carbon nanotubes (CNTs) have been the subject of intense activity;[1] in particular, experiments on transport in CNTs have revealed a wealth of exciting phenomena. Indeed, long metallic CNTs have been shown to behave as quantum wires;[2, 3] negative differential resistance has been observed in semiconducting CNTs.[4] Furthermore, short CNTs have been shown to behave as quantum dots (QDs),[3, 5, 6] exhibiting Coulomb blockade (CB) phenomenology[7] known from gated two-dimensional semiconducting structures.

QDs have spurred a renewed excitement about the Kondo effect (KE), as they allow detailed investigations of the phenomena.[8] In this regard, CNT QDs are ideal for studies of Kondo physics. Indeed, initial experiments displayed an SU(2) KE arising from the electron's spin;[6] more recently, orbital[9] as well as SU(4) KEs have been observed.[9, 10, 11] Furthermore, CNT QDs afford the possibility of tuning between a variety of strongly-correlated (SC) states with a magnetic field.[9, 10]

In this work, we consider transport through CNT QDs, focussing on their behavior in a magnetic field. We analyze the system's evolution from the ultraviolet (UV) to the infrared (IR) fixed points (FPs); we discuss the KEs that arise and their consequences. More specifically, we consider the KEs arising from a single electron (referred to as *1/4-filled*) as well as two electrons (referred to as *1/2-filled*) occupying the energy levels of the CNT QD closest to the Fermi energy E_F of the leads. While previous works detailed the properties of the 1/4-filled QD,[12] we show that the KEs arising from the 1/4-filled and 1/2-filled QDs are drastically different; these differences have pronounced observable consequences.

In what follows, we will be interested in the system's low-energy physics; hence, we focus on the energy levels of the CNT QD closest to E_F of the leads. In the absence of magnetic fields, there are two degenerate energy levels,[9, 13] which we label as α and β . The Hamiltonian we consider is

$$H_{\text{QD}} = \frac{E_C}{2} \left(\hat{N} - N_0 \right)^2 - \frac{h_0}{2} \sum_s (\hat{n}_{\alpha s} - \hat{n}_{\beta s}) \quad (1)$$

$$+ \sum_{\kappa, s} \left(\left[t_1 \psi_{1\kappa s}^\dagger(0) + t_2 \psi_{2\kappa s}^\dagger(0) \right] d_{\kappa s} + \text{h.c.} \right),$$

where $\psi_{i\kappa s}^\dagger(0)$ creates an electron (at $x=0$) with spin- s in band- κ from lead- i ($i=1,2$); $d_{\kappa s}^\dagger$ creates an electron with spin- s in orbital- κ ($\kappa=\alpha,\beta$) on the QD; $\hat{n}_{\kappa s}=d_{\kappa s}^\dagger d_{\kappa s}$

and $\hat{N}=\sum_{\kappa, s} \hat{n}_{\kappa s}$; N_0 is the optimal number of electrons on the QD, which can be controlled by a gate voltage; E_C is the charging energy; t_i is the tunneling matrix element between lead- i and the QD; h_0 is a magnetic field. In this work, we take the $\{t_i\}$ to conserve the orbital quantum number (which is relevant to the experiments in Refs. 10 and 11);[14] as a result, the system has an SU(4) symmetry when $h_0=0$.^[15] h_0 , which would arise from a magnetic field applied parallel to the CNT's axis, splits the α and β orbitals. Throughout this work, we employ units where $\hbar=1$.

It should be noted h_0 would also give rise to a Zeeman splitting, but this splitting is considerably smaller than the orbital splitting, particularly for larger diameter CNTs. Indeed, the orbital moment μ_{orb} of a 5nm diameter CNT was found to be $\mu_{\text{orb}} \simeq 1.5 \text{ meV/T}$ [13] i.e. $\mu_{\text{orb}} \simeq 26 \mu_B$. [μ_B is the Bohr magneton.] As we will be interested in small fields — $h_0 \sim \mathcal{O}(T_K^{\text{SU}(4)})$, where $T_K^{\text{SU}(4)}$ is given by Eq. 5 — the Zeeman splitting will have very small effects. Therefore, in what follows, we focus on the orbital splitting.

We begin our discussion of the properties of CNT QDs by considering the current $I=\langle \hat{I} \rangle$, where \hat{I} is the current operator

$$\hat{I} = -iet_1 \sum_{\kappa, s} \left[\psi_{1\kappa s}^\dagger(0) d_{\kappa s} - d_{\kappa s}^\dagger \psi_{1\kappa s}(0) \right] \quad (2)$$

(e is the electron's charge); in particular, we compute the conductance $G=dI/dV$ vs. N_0 (in linear response). We are interested in the behavior of G as h_0 is varied, as well as how G evolves (with temperature) from the UV to the IR FPs. To understand the IR behavior, G was computed as per Ref. 16 using the logarithmic-descretization embedded cluster approximation (LDECA)[17] and the Friedel sum rule[18]; to treat the UV regime — $T \gg \Gamma_i$, where $\Gamma_i=2\pi\rho_0 t_i^2$ with ρ_0 being the electrons' density of states in the leads — we employed a master equation approach.[19]

Fig. 1a shows G vs. N_0 in the UV regime for several values of h_0 . Letting $\Gamma_0=2\Gamma_1\Gamma_2/(\Gamma_1+\Gamma_2)$,

$$G = e^2 \Gamma_0 \sum_{\{N_\alpha, N_\beta, N'_\alpha, N'_\beta\}} \max\{M_{N_\alpha N_\beta}, M_{N'_\alpha N'_\beta}\} P_{N_\alpha N_\beta}$$

$$\times \frac{\exp[(E_{N_\alpha N_\beta} - E_{N'_\alpha N'_\beta})/T] + 1}{8T \cosh^2[(E_{N_\alpha N_\beta} - E_{N'_\alpha N'_\beta})/2T]},$$

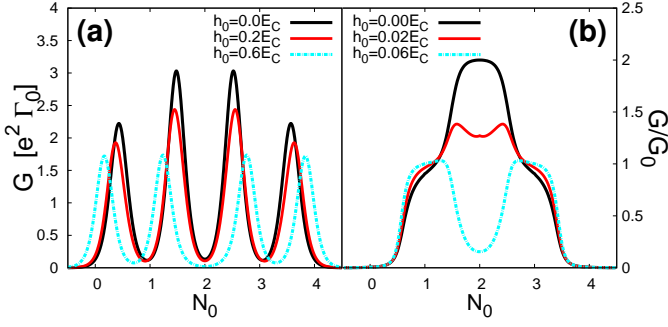


FIG. 1: $G=dI/dV$ vs. N_0 in linear response for several values of h_0 : (a) $T=0.1E_C$ and (b) $T=0$.

where $P_{N_\alpha N_\beta}$ is the probability for the QD to be in a state with N_α (N_β) electrons in the α (β) orbital, $E_{N_\alpha N_\beta}$ is the energy of the state with $M_{N_\alpha N_\beta}$ being the number of these states, and the $\{N_\alpha, N_\beta, N'_\alpha, N'_\beta\}$ satisfy $(N_\alpha + N_\beta) - (N'_\alpha + N'_\beta) = 1$. In Fig. 1a, we observe the well-known CB peaks for $N_0 = N + 1/2$ (N is an integer) and valleys for $N_0 = N$. When $h_0 = 0$, the system has an $SU(4)$ symmetry; the two middle peaks have more spectral weight e.g. the peak at $N_0 = 3/2$ (due to fluctuations between states with $N=1$ and $N=2$) has more spectral weight than the peak at $N_0 = 1/2$ (due to fluctuations between states with $N=0$ and $N=1$). From the above expression for G , this occurs because there are more states with $N=2$ than $N=1$ or $N=0$. When $h_0 \neq 0$, the $SU(4)$ symmetry is reduced to $SU(2)$; as a result, the peaks are split and the spectral weight becomes evenly distributed.

Fig. 1b shows G/G_0 vs. N_0 at $T=0$, where $G_0 = (e^2/\pi)4\Gamma_1\Gamma_2/(\Gamma_1 + \Gamma_2)^2$. Rather than four peaks, we see three distinct plateaus when $h_0 = 0$ — $G/G_0 = 1$ for the plateaus centered about $N_0 = 1$ and $N_0 = 3$; $G/G_0 = 2$ for the plateau centered about $N_0 = 2$. Furthermore, h_0 has interesting effects on G — whereas h_0 mainly splits the peaks in the UV regime (Fig. 1a), h_0 has more drastic effects in the IR. Indeed, the plateau centered about $N_0 = 2$ is suppressed by h_0 ; the plateaus centered about $N_0 = 1$ and $N_0 = 3$, on the other hand, are unaffected. As discussed below, the behavior at $T=0$ occurs because SC states between the QD and leads are formed; h_0 has drastic effects on the SC states.

We now address the physics behind Fig. 1 — we investigate the SC states which arise in the IR, as well as how they evolved from the UV FP. To this end, we examine the QD's spectral function (SF), $A_d(\omega)$. Fig. 2 shows $A_d(\omega)$ (at $T=0$) obtained via the LDECA. For comparison, results for $A_d(\omega)$ at the UV FP — obtained by formally setting $\{t_i\} = 0$ — are shown in the insets. Fig. 2a shows $A_d(\omega)$ at the $N_0 = 1/2$ CB peak. Here we see a broad peak near $\omega = 0$ i.e. near E_F ; its features do not change much with h_0 . From the insets, we see there was a redistribution of spectral weight, with much of the peak's weight in the IR having been transferred from higher energies.

Figs. 2b and 2c show $A_d(\omega)$ in the CB valleys. A key feature is the narrow resonance which appears at or near E_F — the Kondo resonance (KR). This resonance is a consequence of the SC state formed between the QD and

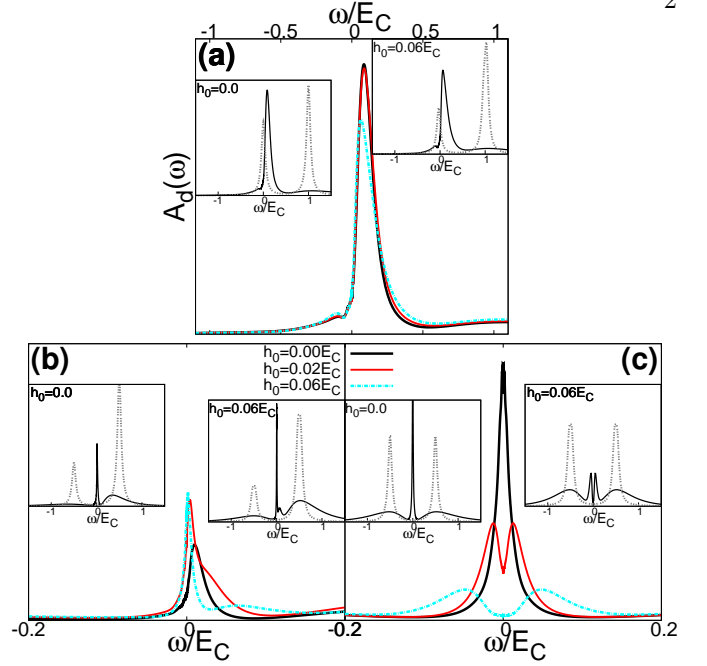


FIG. 2: QD's spectral function $A_d(\omega)$. (a) $A_d(\omega)$ for $N_0 = 1/2$. (b) $A_d(\omega)$ for $N_0 = 1$. (c) $A_d(\omega)$ for $N_0 = 2$. Insets: Comparison of $A_d(\omega)$ at the UV (gray dotted lines) and IR (solid black lines) fixed points.

leads due to the KE; its width represents the dynamically generated scale characteristic of the SC state — the Kondo temperature, T_K . As discussed below, the position and width of the KR are characteristic of the particular Kondo fixed point (KFP).

Fig. 2b shows $A_d(\omega)$ in the $N_0 = 1$ valley i.e. the $1/4$ -filled QD. For $h_0 = 0$, $A_d(\omega)$ exhibits a KR near E_F ; for $h_0 \neq 0$, the resonance moves toward E_F and its width narrows. As mentioned above, when $h_0 = 0$ the system has an $SU(4)$ symmetry; $h_0 \neq 0$ reduces this symmetry to $SU(2)$. For the $1/4$ -filled QD, the system flows to the $SU(4)$ KFP when $h_0 = 0$, while $h_0 \neq 0$ drives the system to the $SU(2)$ KFP; the KR is near (at) E_F at the $SU(4)$ ($SU(2)$) KFP with $T_K^{SU(2)} < T_K^{SU(4)}$. The UV and IR behaviors of $A_d(\omega)$ are compared in the insets — the KR is indeed an IR property, with its spectral weight taken from the higher energy UV peaks; interestingly, h_0 does not change the qualitative features of $A_d(\omega)$ at either the UV or IR FPs.

Fig. 2c shows $A_d(\omega)$ for $N_0 = 2$ i.e. the $1/2$ -filled QD — its behavior is drastically different from the SFs arising for both $N_0 = 1/2$ and $N_0 = 1$. For $h_0 = 0$, $A_d(\omega)$ exhibits a narrow KR at E_F ; for $h_0 \neq 0$, the resonance splits and is suppressed. Hence, contrary to the $1/4$ -filled QD where h_0 drives the system from the $SU(4)$ KFP to the $SU(2)$ KFP, h_0 destroys the KE for the $1/2$ -filled QD. The UV and IR behaviors of $A_d(\omega)$ are compared in the insets — we see the KR suppressed as h_0 increases; as this occurs, the peaks at $\omega = \pm E_C/2$ regain spectral weight.

Having discussed the QD's SF in the various regimes, we now discuss (further) consequences of the SF's features in the CB valleys i.e. for $N_0 \simeq N$. To facilitate the analysis, we integrate out charge fluctuations on the QD;

we arrive at the Coqblin-Schrieffer Hamiltonian[18]

$$H_{\text{QD}} = -\frac{J}{4} \left(\psi_{\kappa s}^\dagger f_{\kappa s} \right) \left(f_{\kappa' s'}^\dagger \psi_{\kappa' s'} \right) - \frac{h_0}{2} f_{\kappa s}^\dagger \sigma_{\kappa \kappa'}^z f_{\kappa' s} \quad (3)$$

where $\psi_{\kappa s} = [t_1 \psi_{1\kappa s}(0) + t_2 \psi_{2\kappa s}(0)]/t$ with $t = \sqrt{t_1^2 + t_2^2}$, $J = (4t^2/E_C) [(N - N_0 - 1/2)^{-1} - (N - N_0 + 1/2)^{-1}]$, and the fermion operators satisfy the constraint $f_{\kappa s}^\dagger f_{\kappa s} = N$ with N being the number of particles on the QD. (While discussing the physics of the CB valleys, we write the QD's fermion operators as $\{f_{\kappa s}\}$; also, Einstein summation convention is utilized). To treat Eq. 3, we consider a path integral representation of the partition function – we enforce the constraint $f_{\kappa s}^\dagger f_{\kappa s} = N$ with a Lagrange multiplier field λ ; we decouple the Kondo interaction using a Hubbard-Stratonovich field χ . [18] We arrive at an effective Hamiltonian

$$H_{\text{eff}} = -\frac{h_0}{2} f_{\kappa s}^\dagger \sigma_{\kappa \kappa'}^z f_{\kappa' s} + \lambda (f_{\kappa s}^\dagger f_{\kappa s} - N) \quad (4)$$

$$+ \frac{4}{J} |\chi|^2 + \chi^\dagger f_{\kappa s}^\dagger \psi_{\kappa s} + \chi \psi_{\kappa s}^\dagger f_{\kappa s}.$$

We begin by considering the physics at higher energies, focussing on the flow from the UV to the IR FPs. To do so, we treat the Bose fields χ and λ in Eq. 4 in mean-field theory (MFT). Treating λ in MFT amounts to treating the constraint $f_{\kappa s}^\dagger f_{\kappa s} = N$ on average: $\langle f_{\kappa s}^\dagger f_{\kappa s} \rangle = N$. To describe the physics near the UV FP, we take $\langle \chi \rangle = 0$; the physics of the KE is contained in the effective action for χ , obtained by integrating out the f -fermions and leads. To one-loop order, the propagator of the χ field $\mathcal{J}(i\omega_m)$ is given by the diagram in Fig. 3 (with ω_m being a boson Matsubara frequency). Physically, $\mathcal{J}(i\omega_m)$ is the running Kondo coupling.[20]

Using our result for $\mathcal{J}(i\omega_m)$, the current $I = \langle \hat{I} \rangle$ was computed as per Ref. 16; results for G/G_0 vs. $T/T_K^{\text{SU}(4)}$ are shown in Fig. 4, where

$$T_K^{\text{SU}(4)} = D \exp(-1/\rho_0 J) \quad (5)$$

with D being half the leads' bandwidth. [As before, $G_0 = (e^2/\pi) 4\Gamma_1 \Gamma_2 / (\Gamma_1 + \Gamma_2)^2$.] Fig. 4a shows results for the 1/4-filled QD. To begin with, we see that G grows logarithmically as T is reduced — this is a consequence of the logarithmic growth of the running Kondo coupling.[18] Furthermore, G/G_0 always grows to $\mathcal{O}(1)$ i.e. the system always flows to strong coupling. This is because the 1/4-filled QD exhibits a KE, irrespective of the value of h_0 . However, G grows more slowly for larger h_0 — the system flows to the SU(4) (SU(2)) KFP for smaller (larger) h_0 ; the slower growth of G for larger h_0 occurs because $T_K^{\text{SU}(2)} < T_K^{\text{SU}(4)}$. (See Fig. 2b.)

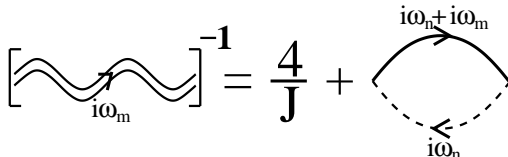


FIG. 3: χ field propagator $\mathcal{J}(i\omega_m)$ — the solid (dashed) line denotes the leads' (f -fermions') Green's function.

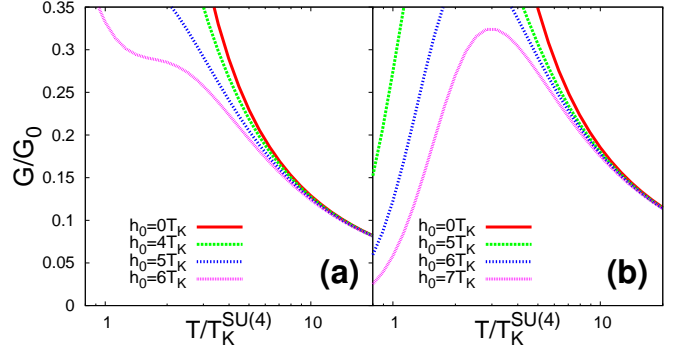


FIG. 4: G/G_0 vs. $T/T_K^{\text{SU}(4)}$ in linear response in the CB valleys: (a) 1/4-filled QD and (b) 1/2-filled QD.

Fig. 4b shows G/G_0 vs. $T/T_K^{\text{SU}(4)}$ for the 1/2-filled QD; the results are drastically different from the 1/4-filled QD. As discussed above, whereas h_0 drives the system from the SU(4) to the SU(2) KFP for the 1/4-filled QD, h_0 destroys the KE for the 1/2-filled QD (see Fig. 2c); G even becomes non-monotonic. Such behavior has been observed in magnetic alloys, where the occurrence of a spin glass phase freezes spin-flip processes and, hence, suppresses the KE.[21] Here, larger values of h_0 freeze both spin and orbital processes. More precisely, h_0 cuts off the growth of the running Kondo coupling — for the 1/2-filled QD $\mathcal{J}(T) \equiv \mathcal{J}(i\omega_m=0)$ is given by

$$\rho_0 \mathcal{J}(T) = J \left\{ \ln \left(\frac{2\pi T}{T_K^{\text{SU}(4)}} \right) + \text{Re} \left[\psi \left(\frac{1}{2} + i \frac{h_0}{4\pi T} \right) \right] \right\}^{-1},$$

where $\psi(z)$ is the digamma function;[22] as $\psi(z) \simeq \ln(z)$ for $|z| \gg 1$, the growth of $\mathcal{J}(T)$ is suppressed for h_0 sufficiently larger than $T_K^{\text{SU}(4)}$.

Having discussed the flow (in the CB valleys) from the UV to the KFPs in the IR, we now discuss further the physics of the SC KFPs. As before, we treat the Bose fields in Eq. 4 in MFT. Now, however, to describe the physics of the SC KFPs, we take $\langle \chi \rangle = \chi_0 (\neq 0)$. [18] Hence, λ and χ_0 are determined via $\langle f_{\kappa s}^\dagger f_{\kappa s} \rangle = N$ and $\chi_0 + 2J \langle \psi_{\kappa s}^\dagger f_{\kappa s} \rangle = 0$. With $\langle \chi \rangle \neq 0$, the f -fermions SF is

$$A_i^f(\omega) = \frac{2\Gamma}{(\omega - \varepsilon_i)^2 + \Gamma^2}$$

($\varepsilon_{1/2} = \lambda \pm h_0/2$), where $\Gamma = T_K$ when $T=0$. [18]

Fig. 5 shows G/G_0 vs. $h_0/T_K^{\text{SU}(4)}$ (computed as per Ref. 16) at $T=0$. For the 1/4-filled QD, $G/G_0=1$ regardless of the value of h_0 . This occurs because there is always a KE, $\Gamma \neq 0$ — for small h_0 , one is in the SU(4) Kondo regime; for larger h_0 , one crosses over to the SU(2) Kondo regime. For the 1/2-filled QD, on the other hand, we see that G depends on the magnitude of h_0 — $G/G_0=2$ for $h_0=0$ and decreases as h_0 is increased. [Within MFT, $G \rightarrow 0$ for $h_0=2T_K^{\text{SU}(4)}$.] This is because the SU(4) KE is destroyed and, consequently, the KR in the QD's SF is suppressed for h_0 sufficiently large. (See Fig. 2c.)

Also shown in Fig. 5 are results for the noise (which has been shown to be a powerful probe of Kondo physics[23,

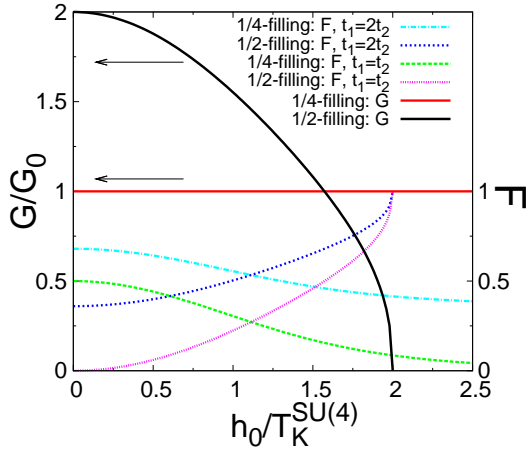


FIG. 5: G/G_0 vs. $h_0/T_K^{\text{SU}(4)}$ and F vs. $h_0/T_K^{\text{SU}(4)}$ in linear response at $T=0$.

24]) at $T=0$. More specifically, we computed the zero-frequency noise

$$S(\text{eV}) = \int dt \left[\langle \hat{I}(t)\hat{I} \rangle - \langle \hat{I} \rangle^2 \right] \quad (6)$$

and, subsequently, the Fano factor $F \equiv S/2eI$ in linear response. While the conductance probes the spectral weight of the KR, the noise gives information about its position. Indeed, while both the $\text{SU}(4)$ and $\text{SU}(2)$ KEs

give $G/G_0=1$ for the 1/4-filled QD, differences between the two can drastically be seen in F — F decreases as h_0 increases i.e. as we move from the $\text{SU}(4)$ to the $\text{SU}(2)$ KFP. This is seen most dramatically when $t_1=t_2$ where $F \rightarrow 0$ as h_0 increases, but the qualitative behavior of F is robust. [See the results for $t_1=2t_2$.] Physically, this arises because the KR in the QD's SF is at E_F at the $\text{SU}(2)$ KFP, while it is away from E_F at the $\text{SU}(4)$ KFP. (See Fig. 2b.) For the 1/2-filled QD, F increases as h_0 increases, approaching unity as $G \rightarrow 0$; for $t_1=t_2$, $F \rightarrow 0$ as $h_0 \rightarrow 0$. For $h_0=0$, the system is in a SC state, with a KR at E_F ; as a result $F=0$ when $t_1=t_2$. As h_0 is increased, the SC state is destroyed and the system is driven to the weak-coupling regime; hence, $F \rightarrow 1$ i.e. F becomes Poissonian.[25]

To summarize, we considered the behavior of CNT QDs in a magnetic field. We analyzed the evolution of the system from the UV to the IR FPs. We discussed the KEs that occur and their experimental consequences. In particular, the KEs arising for the 1/4-filled and 1/2-filled QDs were shown to be drastically different, with distinct signatures in the system's transport; we are optimistic our results, particularly for the noise,[26] can be observed experimentally. Besides CNT QDs, our results are relevant to double QDs and, more generally, to QDs with two-fold orbital degeneracy.

This work was supported by the NSERC of Canada (MM and EHK), a SHARCNET Research Chair (MM and EHK), and the NSF (DMR - 0710529) (GBM).

-
- [1] For reviews, see C. Dekker, *Physics Today* **52**(5), 22 (1999); *Physics World* **13**(6) (2000); R. Saito, G. Dresselhaus, and M. S. Dresselhaus, *Physical Properties of Carbon Nanotubes* (Imperial College Press, London 1998).
 - [2] S. J. Tans, M. H. Deaverot, H. Dai, A. Thess, R. E. Smalley, L. J. Geerligs, and C. Dekker, *Nature (London)* **386**, 474 (1997); Z. Yao, H. W. Ch. Postma, L. Balents, and C. Dekker, *Nature (London)* **402**, 273 (1999).
 - [3] H. W. Ch. Postma, T. Teepen, Z. Yao, M. Grifoni, and C. Dekker, *Science* **293**, 76 (2001).
 - [4] C. Zhou, J. Kong, E. Yenilmez, and H. Dai, *Science* **290**, 1552 (2000).
 - [5] M. Bockrath, D. H. Cobden, P. L. McEuen, N. G. Chopra, A. Zettl, A. Thess, and R. E. Smalley, *Science* **275**, 1922 (1997); J. Kong, C. Zhou, E. Yenilmez, and H. Dai, *Appl. Phys. Lett.* **77**, 3977 (2000); M. J. Biercuk, S. Garaj, N. Mason, J. M. Chow, and C. M. Marcus, *Nano Lett.* **5**, 1267 (2005).
 - [6] J. Nygard, D. H. Cobden, and P. E. Lindelof, *Nature* **480**, 342 (2000).
 - [7] For a review, see, H. Grabert and M. H. Devoret, Eds., *Single Charge Tunneling* (Plenum, New York 1991).
 - [8] L. Kouwenhoven and L. Glazman, *Physics World* **14**(1), 33 (2001).
 - [9] P. Jarillo-Herrero, J. Kong, H. S. J. van der Zant, C. Dekker, L. P. Kouwenhoven, and S. DeFranceschi, *Nature* **434**, 484 (2005).
 - [10] A. Makarovski, A. Zhukov, J. Liu, and G. Finkelstein, *Phys. Rev. B* **75**, 241407(R) (2007).
 - [11] A. Makarovski, J. Liu, and G. Finkelstein, *Phys. Rev. Lett.* **99**, 066801 (2007).
 - [12] M. S. Choi, R. Lopez, and R. Aguado, *Phys. Rev. Lett.* **95**, 067204 (2005); J. S. Lim, M.-S. Choi, M. Y. Choi, R. Lopez, and R. Aguado, *Phys. Rev. B* **74**, 205119 (2006).
 - [13] E. Minot, Y. Yaish, V. Sazonova, and P. L. McEuen, *Nature* **428**, 536 (2004).
 - [14] F. B. Anders, D. E. Logan, M. R. Galpin, and G. Finkelstein, *Phys. Rev. Lett.* **100**, 086809 (2008).
 - [15] For a review of $\text{SU}(4)$ KEs in nanostructures, see G. Zarand, *Philos. Mag.* **86**, 2043 (2006).
 - [16] Y. Meir and N. Wingreen, *Phys. Rev. Lett.* **68**, 2512 (1992).
 - [17] E. V. Anda, G. Chiappe, C. A. Büsser, M. A. Davidovich, G. B. Martins, F. Heidrich-Meisner, and E. Dagotto, *Phys. Rev. B* **70**, 085308 (2008).
 - [18] A. Hewson, *The Kondo Effect to Heavy Fermions* (Cambridge University Press, Cambridge 1993).
 - [19] C. W. J. Beenakker, *Phys. Rev. B* **44**, 1646 (1991).
 - [20] P. Coleman, *Phys. Rev. B* **35**, 5072 (1987).
 - [21] See, e.g. F. Schopfer, C. Bäuerle, W. Rabaud, and L. Saminadayar, *Phys. Rev. Lett.* **90**, 056801 (2003).
 - [22] I. S. Gradshteyn and I. M. Ryzhik, *Table of Integrals, Series, and Products* (Academic Press, San Diego 1994).
 - [23] Y. Meir and A. Golub, *Phys. Rev. Lett.* **88**, 116802 (2002); E. Sela, Y. Oreg, F. von Oppen, and J. Koch, *Phys. Rev. Lett.* **97**, 086601 (2006).
 - [24] T. Delattre, C. Feuillet-Palma, L. G. Herrmann, P. Morfin, J.-M. Berroir, G. Feve, B. Placais, D. C. Glattli, M.-S. Choi, C. Mora, and T. Kontos, *Nature Physics* **5**, 208 (2009).

- [25] Ya. M. Blanter and M. Büttiker, Phys. Rep. **336**, 1 (2000).
- [26] Indeed, by working at lower temperatures and in a mag-

netic field, we are optimistic our results for the noise could be observed in the device/setup of Ref. 24.